Appl. Phys. B 68, 383–392 (1999)

Applied Physics B
Lasers
and Optics

Invited paper

Time-resolved coherent spectroscopy of surface states

U. Höfer

Max-Planck-Institut für Quantenoptik, D-85740 Garching, Germany
and Physik Department, Technische Universität München, D-85747 Garching, Germany
(Fax: +49-89/3290-5200, E-mail: Hoefer@mpq.mpg.de)

Received: 4 December 1998

Abstract. Ultrafast electronic coherence phenomena of metallic image-potential states and of silicon dangling-bond states are discussed. The image states were investigated on a Cu(100) surface by means of time-resolved two-photon photoemission (2PPE). Spectroscopical and dynamical information about states with high quantum numbers ($n \geq 4$) were obtained by the coherent excitation of several eigenstates of the Rydberg series and detection of the resulting quantum beats. Electron wave packets that describe the quasi-classical periodic motion of weakly bound electrons at metal surfaces could be created by the superposition of several eigenfunctions around $n = 7$. A surface-sensitive purely optical technique is introduced for the investigation of rapid dephasing processes of excited dangling-bond states of Si(111)7×7. The measurement of the diffracted second-harmonic signal from a transient population grating yielded decoherence times of about 5 fs.

PACS: 42.50.Md; 73.20.-r; 79.60.-i

Lasers have revolutionized time-resolved spectroscopy not only because they allow the generation of the shortest light pulses. Equally important for many applications in atomic, molecular and condensed matter physics has been the fact that they provide an intense coherent source of radiation. There is then a well-defined phase relationship between the wave functions of the states that are coupled by the interaction with the light. Generally, coherent spectroscopic techniques that exploit this phase relationship gain more information than techniques that rely only on the measurement of intensities. Among the most well-known examples are coherent Raman scattering, quantum-beat spectroscopy, and echo and induced grating experiments [1–3].

There are only a few examples where coherence phenomena have been exploited for surface studies. In a pioneering application of picosecond infrared-visible sum-frequency generation, Guyot-Sionnest succeeded in observing the free-induction decay and photon echo of the long-lived stretching vibrations of H/Si(111) and to separate their true homogenous dephasing time from inhomogeneous contributions [4]. Other measurements of free-induction decay of vibrational excitations have been reported for the system CO/Cu [5]. The coherent excitation of surface optical phonons and their detection with optical second-harmonic generation was demonstrated by Chang, Xu, and Tom [6]. Petek and co-workers performed interferometric two-pulse correlation measurements in two-photon photoemission from metal surfaces. They could observe dephasing of hot electrons in Cu(111) on a timescale of the order of 5 fs and demonstrate coherent control of electron emission in a Ramsey-fringe-type experiment [7, 8].

The topic of this paper is coherent phenomena of surface electronic states. In the first part, I am going to give a somewhat extended account of our recently reported investigations of image-potential states with two-photon photoemission (2PPE). In an ordinary time-resolved 2PPE experiment, a short pump laser pulse excites an electron into an intermediate state, a subsequent probe pulse emits it into the vacuum. The kinetic energy and the angle at which the electron leaves the surface are measured and yield information about the energy and the parallel momentum of the intermediate state [9–15]. In the case of high-order image-potential states we have gone one step further and prepared a coherent superposition of several intermediate states by the pump pulse. We were thus able to observe wave-packet dynamics and gain information from quantum beat spectroscopy [16, 17].

In the second part, optical second-harmonic generation (SHG) [18–20] is combined with transient grating techniques to obtain surface-specific information of ultrafast electronic dephasing processes. The five-wave mixing process yields similar information about electron dynamics at surfaces as time-resolved four-wave-mixing investigations about bulk excitations. The method is demonstrated for dangling-bond excitations of Si(111)7×7 that could be well characterized with 2PPE and adsorption experiments. With the wide availability of high-intensity ultra-short laser pulses, the purely optical technique could become a valuable tool for the investigation of ultrafast dynamics at many interfaces.

1 Coherent 2PPE of image-potential states

Image-potential states are a class of normally unoccupied electronic states that exist at the surfaces of many single-crystal metals [21–23]. An electron at a distance z in front of a metal surface induces an electric dipole field and experiences an attractive force, $F(z) = -e^2/(2z)^2$, identical to the one produced by a positive image charge at $-z$ inside the metal (Fig. 1). If the metal has a band gap near the vacuum energy (in the direction perpendicular to the surface) then an electron below E_{vac} may be trapped in the potential well consisting of the Coulomb-like attractive image potential $V(z) = -e^2/4z$ and the repulsive surface barrier [21]. The resulting quantized electronic states form a Rydberg series with energies E_n converging towards the vacuum energy E_{vac}:

$$E_n = E_{\mathrm{vac}} - \frac{0.85\,\mathrm{eV}}{(n+a)^2}\,, \quad n = 1, 2, \ldots \tag{1}$$

In this equation the influence of the surface potential on the binding energy is approximated by a quantum defect $0 \le a \le 0.5$. Because the wave functions of image-potential states are mainly located in the vacuum in front of the surface, the lifetimes associated with image states can be significantly longer than those of electronic excitations in the metal [24, 25].

The image-potential states were investigated for the surfaces of Cu(111), Cu(100) and Ag(100). The preparation of the samples and details of the ultra-high vacuum chamber employed have been described elsewhere [22]. Frequency-tripled ultraviolet (UV) pulses from a 80-MHz femtosecond Ti:sapphire laser with pulse durations between 75 and 95 fs and a photon energy of $\hbar\omega_{\mathrm{a}} = 4.7\,\mathrm{eV}$ were used to excite electrons out of an occupied state below the Fermi energy E_{F} into the image-potential states. The photoelectrons were emitted by the fundamental IR pulses ($\hbar\omega_{\mathrm{b}} = 1.57\,\mathrm{eV}$). They were detected after passing through a hemispherical analyzer with an energy resolution of 30 meV and an angular acceptance of $\pm 0.6^\circ$ about the surface normal. A typical energy-resolved 2PPE spectrum obtained from Cu(100) at room temperature is displayed in Fig. 1. It shows three well-separated peaks corresponding to the emission from the image states with quantum numbers $n = 1, 2, 3$. The coherent phenomena discussed below were investigated for the high-order states ($n > 3$) slightly below the vacuum level. In Fig. 1, these states are only visible as a shoulder at a kinetic energy of ~ 1.5 eV.

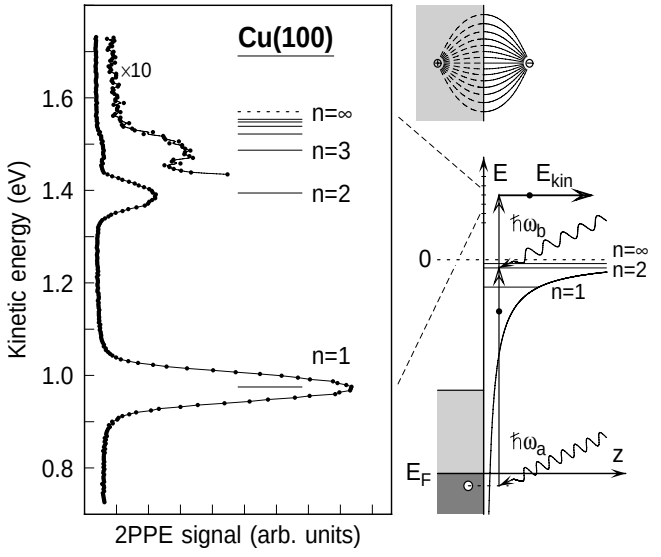

Fig. 1. Energy-resolved 2PPE spectrum of Cu(100) image-potential states and corresponding excitation scheme. The data were taken with zero time delay between the pump pulses ($\hbar\omega_{\mathrm{a}}$) and the probe pulses ($\hbar\omega_{\mathrm{b}}$). The photoelectrons were emitted normal to the surface ($k_{\parallel} = 0$); their kinetic energy is referred to the vacuum level $E_{\mathrm{vac}} \equiv 0$ ($E_{\mathrm{kin}} = \hbar\omega_{\mathrm{b}} + E_n$)

1.1 Dynamics of low-n states

Before we discuss the dynamics of these high-order states it is instructive to have a look at the relaxation behavior of the states $n = 1, 2, 3$. For the experiments, the analyzer was set to a fixed electron energy and the 2PPE intensity was recorded as a function of the variable time delay between the UV pump and the IR probe pulses. The decay times deduced from the correlation traces plotted in Fig. 2 are $\tau_1 = 40 \pm 6$ fs, $\tau_2 = 120 \pm 10$ fs and $\tau_3 = 300 \pm 15$ fs. In a simplified picture, the lifetimes τ_n of the image-potential states are given by the penetration of the wavefunction into the bulk and the decay time of excited bulk states of energy E_n due to electron–hole-pair creation [22]. Recent theoretical results that are in good agreement with our experimental values for τ_n show that there is also a substantial near-surface vacuum contribution to the decay [26]. Both contributions, however, are expected to scale

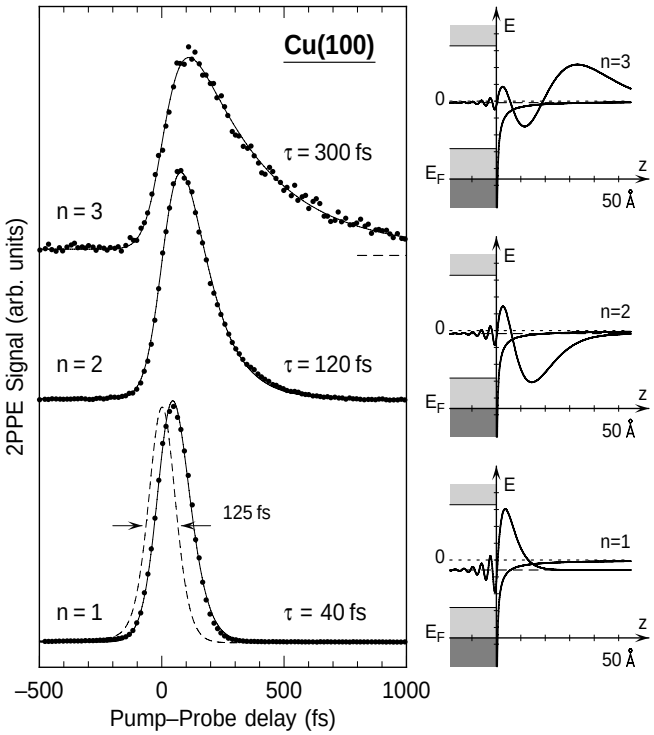

Fig. 2. 2PPE cross-correlation traces obtained for the three lower image-potential states of Cu(100). *Dots* represent data points; *solid lines* are results from density matrix calculations with the intermediate state lifetimes as indicated [27]. The *dashed line* marks the true cross-correlation between pump and probe pulses, which was taken in situ by recording the direct 2PPE signal from the occupied surface state of Cu(111). The penetration of the wave functions of the states $n = 1, 2, 3$ into the s-p band gap of Cu(100) is illustrated at the right

like n^3 in the limit of high n as the overlap of the wavefunctions $|n\rangle$ with the surface region decreases with n^3 [21]. Our results for Cu(100) and Ag(100) show that this power law is indeed valid for $n \geq 2$ [27].

1.2 Quantum beat spectroscopy

The data of Fig. 2 correspond to the decay of a single eigenstate. The low-lying image states are well separated and simultaneous excitation cannot occur for excitation pulses of 95 fs duration. The situation already becomes different when slightly shorter UV pulses are used and the energy analyzer is set to detect two-photon photoemission corresponding to a binding energy below the $n = 3$ state. Results obtained for a pump pulse duration $\tau_{\mathrm{UV}} = 75$ fs and a binding energy $E_{\mathrm{B}} = -E_n = 70$ meV are plotted in Fig. 3. The data show an overall decay of the intensity as a function of the pump–probe delay on a timescale that is similar to the relaxation time of the $n = 3$ state. This overall decay is superimposed by weak oscillations with a periodicity of 115 fs that is clearly revealed after a smoothly decaying curve is subtracted from the data.

This experiment represents a variant of the well-known *quantum beat spectroscopy* of closely adjacent states [28]. Our 75-fs pump pulses have a bandwidth of 30 meV (measured full width at half maximum) and are thus able to coherently excite more than one eigenstate of the Rydberg series. In the simple case of the coherent excitations of two levels n and $n+1$ the oscillations reflect the beating between the corresponding wavefunctions $\Psi_n(t) = |n\rangle \exp(-\mathrm{i}\omega_n t)$ and $\Psi_{n+1}(t) = |n+1\rangle \exp(-\mathrm{i}\omega_{n+1} t)$, with $\omega_n = E_n/\hbar$. Provided there is no loss of coherence, the 2PPE intensity $I(t)$ long after the pulse will be given by

$$I(t) \propto |a_n(t)\Psi_n(t) + a_{n+1}(t)\Psi_{n+1}(t)|^2 \tag{2}$$

$$\propto a_n^2 + a_{n+1}^2 + 2a_n a_{n+1} \cos(\omega_{n,n+1} t) \tag{3}$$

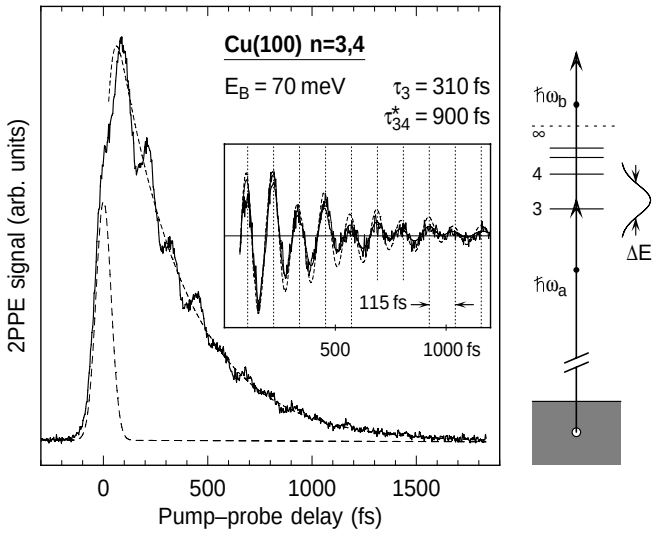

Fig. 3. 2PPE cross-correlation trace obtained for a binding energy that is slightly less than that of the $n = 3$ state by using an excitation pulse of 75 fs duration and a 45-fs IR probe pulse. The weak coherent admixture of the $n = 4$ state leads to periodic oscillations of the 2PPE signal as a function of pump–probe delay (inset). The decay of these quantum beats is only slightly faster (*thin solid line*) than expected from the decay of the population of both states (*dashed line*); it corresponds to a pure dephasing time $\tau^*_{34} = 900$ fs [17]

with the (exponentially) decaying coefficients $a_n(t)$ and $a_{n+1}(t)$ and a beat frequency of $\nu_{n,n+1} = \omega_{n,n+1}/2\pi = (E_{n+1} - E_n)/h$. The beating period of 115 fs in Fig. 3 corresponds to an energy difference of 36 meV.

The quantum beats become much more pronounced when the energy analyzer is set to detect electrons with yet smaller binding energies. An example corresponding to a binding energy $E_{\mathrm{B}} \simeq 40$ meV is displayed in Fig. 4. In this case the almost transform-limited 95-fs sech^2 pump pulse predominantly excites electrons into the $n = 4$ and the $n = 5$ states. The beating period observed for short delays is $\nu^{-1}_{4,5} = 230$ fs. After 2 ps most of the population in the $n = 4$ state has decayed. The oscillations now reflect the interference of the amplitudes in $n = 5$ and the weakly excited $n = 6$ state, which persist at these delays ($\nu^{-1}_{5,6} = 430$ fs). In general, the Fourier transform of the raw data with the smooth exponential decay subtracted directly yields the various beating frequencies. This is shown in the upper right corner of Fig. 4. The two main frequency components are 4.3 and 2.3 THz, which yield energy differences of 17.8 meV and 9.6 meV, respectively. The deduced values are slightly higher than the theoretical energy differences expected from (1) with the quantum defect $a = 0.21$ that reproduces the experimental binding energy for the $n = 1$ state.

It must be emphasized that the accurate spectroscopy of these states in the energy domain would require a resolution in the meV range, which is difficult to achieve experimentally. In the literature on image-potential states, for example, the best energy resolution has been reported by Padowitz et al. [29]. With a time-of-flight electron analyzer these authors

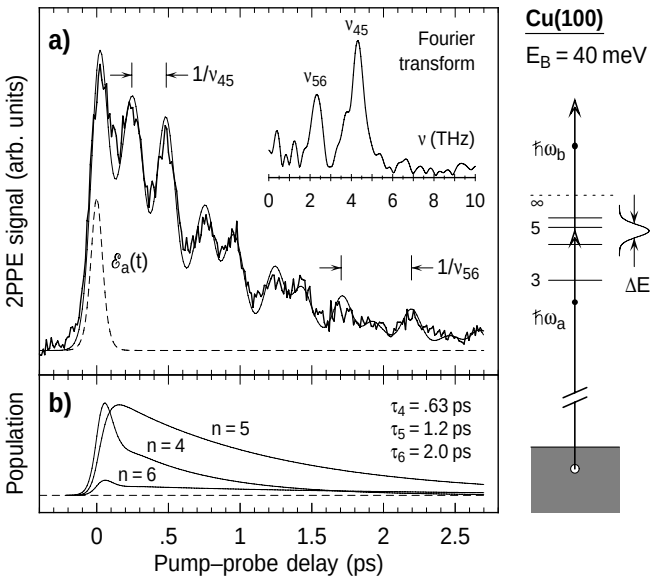

Fig. 4a,b. Quantum beats observed after the coherent excitation of image-potential states with quantum numbers $n = 4, 5, 6$ ($E_{\mathrm{B}} \simeq 40$ meV). **a** The *thick curve* corresponds to the measured 2PPE signal as a function of pump-probe delay. The *thin line* is the result of the density matrix calculation for the two-photon excitation depicted schematically on the right-hand side of the figure. The *dashed line* shows the envelope $\mathcal{E}_a(t)$ of the exciting UV pulse. The Fourier transform was obtained after subtraction of a smooth exponential decay from the measured data and directly gives the beating frequencies $\nu_{45} = (E_5 - E_4)/h$ and $\nu_{56} = (E_6 - E_5)/h$ between the excited states. **b** Relative population of the individual levels resulting from the calculation and corresponding decay times τ_n. (From [15])

were able to resolve the $n = 4$ state of Xe/Ag(111). With quantum beat spectroscopy, closely separated lines can even be resolved in cases where inhomogeneous broadening of a whole set of levels would principally prevent their spectral resolution. Additionally, time-resolved coherent spectroscopy is able to provide information about the relaxation behavior of the electrons in these states.

A density matrix formalism has been used to quantitatively model excitation, decay, and interference of the image-potential states in a unified way. Briefly, an initial state $|0\rangle$ is coupled to several excited states $|n\rangle = |3\rangle, |4\rangle, \ldots$ by the pump pulse; these are then coupled to a final state $|f\rangle$ by the probe pulse. The decay of the excited states is taken into account by lifetimes τ_n of the population in each state. In order to limit the number of free parameters, the following approximations are made for the present application. (1) Dephasing without population decay (pure dephasing) is neglected. (2) Power laws are assumed for lifetimes $\tau_n \propto (n + a)^3$ and coupling strength $\frac{i}{\hbar}\langle n|\mu_a|0\rangle \propto (n + a)^{-3}$. (3) All energies of excited states are assumed to be given by (1). (4) The coupling of the excited states to the continuum by the probe pulse is approximated by a weighted projection of the coherent superposition of excited states into the continuum and convolution with the envelope of the probe pulse. A Gaussian analyzer transmission function, with a power law for the emission probability $\frac{i}{\hbar}\langle f|\mu_b|n\rangle \propto (n + a)^{-3}$, is used to describe the detection probability. (5) An important effect to obtain close quantitative agreement with the experiment is the availability of a continuum of initial states in the conduction band of the metal and the finite energy resolution of the electron analyzer. It is taken into account by performing the calculation for different initial states and by incoherently summing up the obtained intensities.

A fit of the model calculation with excited states from $n = 4, \ldots, 8$ taken into account is shown in Fig. 4a. Apart from a trivial scaling factor, the fit has only three variable parameters: the lifetime τ_4, the quantum defect a and the mean binding energy of the detected states E_B. Although the last of these is fixed by the experiment, we observed that the modelling is more sensitive to this parameter than to the accuracy with which we could control it experimentally (± 10 meV). In view of the approximations involved and the few variable parameters in the fit, the agreement between the experiment and the theoretical model is excellent and confirms the validity of the theoretical description. The deduced quantum defect is $a = 0.15$. The lifetime of the $n = 4$ state is $\tau_4 = 630$ fs, which is only slightly smaller than the 690 fs obtained by extrapolating from $\tau_3 = 300$ fs with the $(n + a)^3$ power law. The observed slight deviations of the level spacing from the behavior predicted by (1) and the exact dependences of the lifetimes of the image states on the quantum number are related to the details of the electronic structure of the surface [22]. The lower part of the figure displays the calculated population in the states $n = 4, 5, 6$ that mainly contribute to the measured intensity. The coherent peaks visible for $n = 4$ and $n = 6$ are caused by off-resonant excitation of these levels from the continuum of initial states in the metal. The deduced lifetimes are likely to be the longest that have ever been observed for an electronic excitation on a bare metal surface. For example, $\tau_4 = 630$ fs corresponds to a Lorentzian linewidth of $\Gamma \simeq 1$ meV. Of course, the long lifetimes are associated with weak overlap with bulk electronic states. The resulting low excitation cross sections have prevented the time-resolved detection of states beyond $n = 2$ and the energy-resolved detection of states beyond $n = 4$ in previous experiments [22–24, 29].

1.3 Electron wave packets

As the level spacing of the image-potential states decreases with increasing quantum number n, their population with a 95-fs pulse leads to the coherent superposition of 5 or more states. A discussion of the resulting effects in terms of quantum beats would be very complicated and not useful for the understanding of the dynamics of these weakly bound electrons. Instead, a description in terms of a spatially localized wave packet is more appropriate.

In space representation the eigenstates $|n\rangle$ of the image potential are given by the s-like radial wave function of the hydrogen atom $R_n^{l=0}(z)$ multiplied by z and expanded by a factor of 4 [21]. The coherent excitation of several states in the vicinity of some central state $\overline{n}$ out of the initial state localized at the surface creates a wave packet

$$\Psi_{WP}(z, t) = \sum_n a_n z R_n^{l=0}(z/4) e^{-i\omega_n t} . \quad (4)$$

The temporal and spatial evolution of the probability $|\Psi_{WP}(z, t)|^2$ resulting from calculated coefficients $a_n \propto (n + a)^{-3}$ are displayed in Fig. 5 and in the inset of Fig. 6 for two cases. In the case of the superposition of three levels in the vicinity of $\overline{n} = 5$ by a 95-fs pulse the probability $|\Psi_{WP}(z, t)|^2$ concentrates at a distance of ~ 90 Å from the surface (Fig. 5). There, it exhibits only weak temporal modulations that are opposite in phase to the much more pronounced modulations close to the surface. This example corresponds to the quantum beats depicted in Fig. 4. The spatial dynamics of the wave

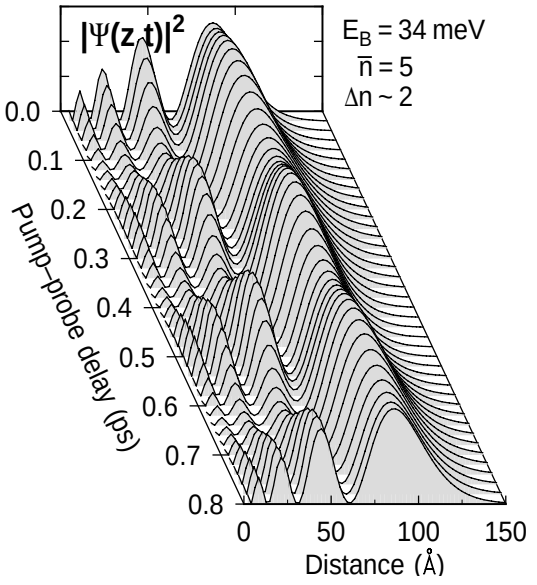

Fig. 5. Calculated temporal evolution of the wave packet created by the coherent superposition of three image-potential states in the vicinity of $\overline{n} = 5$ by a 95-fs pulse. The probability $|\Psi_{WP}(z, t)|^2$ is concentrated at a distance of $z \sim 90$ Å from the surface and exhibits only a weak temporal modulation. The variations near the surface are reflected in the oscillations of the measured 2PPE signal (compare Fig. 4)

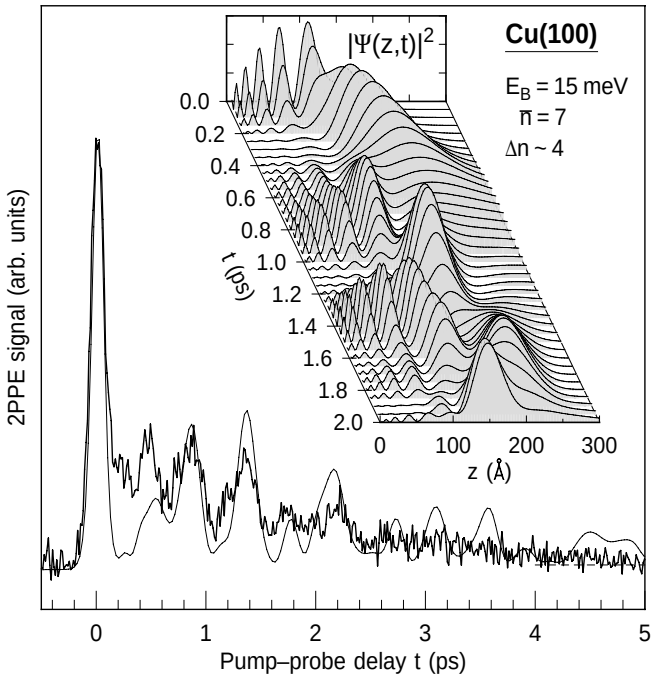

Fig. 6. Wave-packet excitation of weakly bound image-potential states centered around $\overline{n} = 7$ ($E_B \simeq 15$ meV). *Thick lines* in the main panel indicate the recorded 2PPE signal as a function of the delay t of the IR probe pulse with respect to the exciting UV pulse. The smooth thin line is the intensity calculated by assuming excitation from a single initial state. The inset shows the corresponding temporal and spatial evolution of the created coherent state for the first 2 ps. (After [15])

packet is negligible for the description of this experiment. When the same pulse excites image-potential states in the vicinity of $\overline{n} = 7$, five levels ($n = 5, \ldots, 9$) appreciably contribute to the total amplitude. The wave packet now displays much more dramatic spatial dynamics. The probability of locating the electron oscillates back and forth from the surface (Fig. 6, inset).

For the further discussion it is instructive to note that in the classical limit the orbiting period of an electron is given by $T_n = 2\pi/(\omega_{n+1} - \omega_n)$. A Taylor expansion of $\omega_n \propto n^{-2}$ around the central frequency $\omega_{\overline{n}}$ then becomes

$$\omega_n = \omega_{\overline{n}} + \frac{2\pi}{T_{\overline{n}}}\Delta n - \frac{2\pi}{(2\overline{n}/3)T_{\overline{n}}}(\Delta n)^2 + \ldots \qquad (5)$$

where $\Delta n = n - \overline{n}$. When only the harmonic term of (5) is considered, the wave function (4) can be written in terms of product of a fast oscillating contribution that is not observable in the experiment and a term with a periodicity of the classical revolution time $T_{\overline{n}}$

$$\Psi_{\mathrm{WP}}(z,t) = \mathrm{e}^{-\mathrm{i}\omega_{\overline{n}}t}\sum_n a_n z R_n^{l=0}(z/4) \times \exp\left[-2\pi i\left(\frac{\Delta n t}{T_{\overline{n}}} + \ldots\right)\right]. \qquad (6)$$

The inset of Fig. 6 shows that immediately after the excitation ($t \simeq 0$) the electron has a high probability of being located close to the surface. $|\Psi_{\mathrm{WP}}|^2$ exhibits the minima and maxima typical for the Laguerre polynomials that constitute the individual eigenfunctions $|n\rangle$ which according to (6) all add in phase. As time progresses the individual $|n\rangle$s get out of phase and the center of mass of $|\Psi_{\mathrm{WP}}|^2$ moves away from the surface. After $t = T_{\overline{n}}/2 \simeq 0.4$ ps the wavefunction of neighboring states are added with opposite signs. The amplitudes near the surface have completely disappeared and Ψ_{WP} describes an electron located almost 200 Å away from the surface. The process then repeats itself with a period of $T_{\overline{n}} \simeq 0.8$ ps. Because of the significant dispersion of the levels described by the higher terms in the Taylor expansion (5), this repetition is not exact, and the electron becomes delocalized for $t > 2$ ps (not shown).

Results corresponding to such a situation were obtained by performing 2PPE experiments for a binding energy of $E_B \simeq 15$ meV. The excited eigenstates are centered around $\overline{n} = 7$. The data displayed in the main panel of Fig. 6 show a strong correlation feature at delay zero and oscillations that persist for more than 3 ps. The smooth line is the result of the density matrix calculation with intermediate states between $n = 4$ and $n = 15$ taken into account. In order to reveal the main features, the effect of the incoherent summation over different excitations due to the limited energy resolution has been neglected. Nevertheless, the calculation qualitatively reproduces the main experimental features quite well.

A comparison of the temporal evolution of the wave packet reproduced in the inset of Fig. 6 and the 2PPE intensity shows that the second laser pulse probes the localization of the oscillating electron. The distance of the wave packet from the surface is reflected in the strength of the 2PPE signal. For example, the minima at $t = 1.1$ and 1.6 ps and the maxima at 0.9 and 1.4 ps are clearly correlated with the wave-packet motion. Deviations between experiment and calculation are mainly caused by the limited energy resolution of the electron analyzer (30 meV compared to a bandwidth of the excitation pulse of 14 meV). For this reason, not all of the detected photoelectrons originate from the coherent excitation of the same intermediate levels.

Qualitatively, the detection of the wave packet motion by the probe pulse can be understood from the fact that far away from the surface the electron is nearly free and cannot absorb a photon. Only if it is close to the surface, the metal is able to provide the necessary momentum for photon absorption. Quantitatively, the larger photoemission matrix element close to the surface is related to the potential gradient $\nabla_z V$ [30].

Our experiments were not the first ones to detect the wave-packet dynamics of electrons. A decade ago it was already possible to use picosecond pulses to create a coherent superposition of atomic Rydberg states with high principal quantum numbers n [32, 33]. The wave packets, which have low angular momentum, correspond to a kind of breathing mode [34] but not to the classical limit of the atom with an orbiting electron [35]. It is a distinct feature of the present experiment that the wave-packet dynamics corresponds to the classical motion of a weakly bound electron in front of a (reflecting) metal surface (Fig. 7). Since the image-state electrons are free to move parallel to the surface and the angle-resolved detector used for the 2PPE experiment selects an electron with well-defined parallel momentum $\hbar k_\parallel$ the time axis of Fig. 6 (inset) can be read as a surface coordinate in the case of off-normal detection $[x(t) = x_0 + (\hbar k_\parallel/m)t]$. For a slighly off-normal emission of $\theta = 1°$, e.g., the parallel velocity of the image-state electron is $\hbar k_\parallel/m = \sqrt{2E_{\mathrm{kin}}/m}\sin\theta \simeq 0.13$ Å/fs.

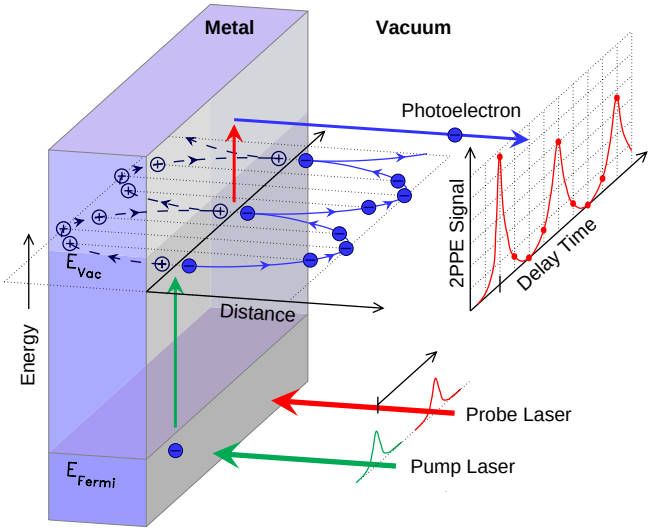

Fig. 7. Simplified quasi-classical scheme of the 2PPE experiment of weakly bound image-potential states. As the parallel velocity of the electron is constant, the oblique direction may be viewed as a surface coordinate or as the time axis. (After [31])

1.4 Dephasing

In the discussion above we have assumed that the phase relationship between the coherently excited eigenstates remains fixed after the excitation pulse is over. Their quantum interference is destroyed only due to the inelastic processes that cause the population to decay as a function of time. In a real system there will also be scattering with surface phonons or defects that involves only small energy transfers [36, 37]. Although the electron stays in the image state the macroscopic coherence of the excited-state wavefunction gets lost when such quasielastic scattering events occur. Our results suggest that for well-prepared surfaces these *dephasing* processes are not very important. They would lead to a decay of the quantum beats that is much faster than the population decay. Analysis of the data from Figs. 3 and 4 shows that this is obviously not the case.

However, when defects are present on the surface, the situation changes dramatically. In a systematic study of the effect of CO adsorbates it was found, for example, that a CO coverage of 4% of a monolayer already causes rapid dephasing of the quantum beats between $n = 3$ and $n = 4$ within 60 fs [27]. For higher CO coverage, quantum beats like the ones shown in Fig. 3 are hardly detectable, although the population decay is comparatively little affected by the presence of the CO adsorbates. Cu adatoms, on the other hand, lead to both rapid dephasing and population decay. For further discussion the reader is referred to the paper by Weinelt et al. in this issue [38].

2 Diffraction of SHG from a transient grating of excited dangling bonds

As time-resolved spectroscopy for surface studies, two-photon photoemission stands out by the excellent characterization of energy and momentum of the excited intermediate state, achieved by analyzing the energy and emission angle of the photoemitted electron. However, the technique is restricted to surfaces in UHV environments. Moreover, it is difficult to apply under the conditions of high excitations densities that are frequently required to investigate the dynamics of chemical or structural changes of surfaces. Such conditions may lead to unwanted electron emission by multiphoton absorption of the pump pulse that destroys the energy and momentum resolution due to space-charge effects [10].

Purely optical techniques like second-harmonic generation (SHG) and sum-frequency generation (SFG) [19], on the other hand, can be applied under these circumstances. However, transient nonlinear optical effects are sometimes difficult to interpret microscopically and few studies have focused on the electron dynamics of surfaces [39–41]. Up to now, electronic coherence effects have mainly been discussed in terms of (unwanted) artifacts in SHG/SFG pump–probe experiments of vibrational energy relaxation or desorption processes of adsorbates [42, 43].

In this section, we are going to discuss an extension of SHG that is *aimed* at the investigation of ultrafast coherent processes at surfaces and interfaces. Two short interfering laser pulses create a transient population grating at a surface which leads to a spatial modulation of its nonlinear susceptibility $\chi_s^{(2)}$ and cause a third pulse to generate SH radiation in diffraction, which is then detected. In the terminology of nonlinear optics, the technique is a five-wave-mixing process characterized by a $\chi^{(4)}$ tensor and as such it is intrinsically surface sensitive on centrosymmetric materials. For a first demonstration, we have excited the dangling bonds of a Si(111)7×7 surface and measured the dephasing of this excitation due to electron–electron scattering on a 10-fs time scale.

2.1 Diffraction from transient surface gratings

Transient gratings have been widely used for the coherent spectroscopy of semiconductors and of molecules in liquid solutions [2, 3]. Two synchronized pump pulses of frequency ω and wave vectors $\boldsymbol{k}_\mathrm{a}$ and $\boldsymbol{k}_\mathrm{b}$ produce the electronic excitation. The grating results from the interference of the two beams, which gives rise to spatial modulation of the linear absorption. In the case of a surface experiment, the beams incident in the x-z plane (x denoting a direction parallel, z perpendicular to the surface) create a grating with k vector $k_\mathrm{G} = k_{\mathrm{b},x} - k_{\mathrm{a},x}$. A synchronized probe pulse of the same frequency ω and wave vector $\boldsymbol{k}_\mathrm{p}$ is Bragg scattered from the transient grating into a direction determined by $k_{\mathrm{d},x} = k_{\mathrm{p},x} \pm k_\mathrm{G}$. The intensity of the diffracted beam depends on the time delay between the various pulses and the relaxation behavior of the electronic system.

The situation becomes most transparent for a resonantly excited two-level system with transition frequency $\omega_{01} = \omega$ in the limit of weak excitation. In this case it is sufficient to calculate the induced polarizations P and population changes N_{01} in the lowest order of the field E from a density-matrix description [3, 44].

$$\frac{\partial}{\partial t} P_j^{(1)} = \frac{i\mu}{\hbar} E_j - \frac{1}{T_2} P_j^{(1)}, \quad j = \mathrm{a,b} \tag{7}$$

$$\frac{\partial}{\partial t} N_{01}^{(2)} = \frac{i\mu}{\hbar} \left(E_\mathrm{a} P_\mathrm{b}^{*(1)} - P_\mathrm{a}^{(1)} E_\mathrm{b}^* \right) + \mathrm{c.c.} - \frac{1}{T_1} N_{01}^{(2)} \tag{8}$$

$$\frac{\partial}{\partial t}P_{\mathrm{d}}^{(3)} = -2\frac{i\mu}{\hbar}E_{\mathrm{p}}N_{01}^{(2)} - \frac{1}{T_2}P_{\mathrm{d}}^{(3)} \tag{9}$$

The first two equations show that the spatial modulation of the population is *not* generated directly by an intensity grating of the interfering pump pulses but by the interference of the polarization induced by one excitation pulse with the field of the other. For the generation of the population grating $N(x) = N_{01}^{(2)}\cos(k_{\mathrm{G}}x)$, whose amplitude $N_{01}^{(2)}$ is assumed to decay exponentially with time constant T_1. It is thus not necessary that the two excitation pulses overlap in time. Instead $N_{01}^{(2)}$ depends on the ratio of the time delay between the pulses $|t_{\mathrm{b}} - t_{\mathrm{a}}|$ and the dephasing time of the polarization T_2. The polarization $P_{\mathrm{d}}^{(3)}$ induced by the interaction of the probe pulse with the grating gives rise to the diffracted radiation of frequency ω by dipole emission.

$P_{\mathrm{d}}^{(3)}(\omega)$ is of third order in terms of the incident fields and thus not surface specific. Instead of the fundamental frequency ω of the diffracted pulse we detect its second-harmonic frequency 2ω. This radiation originates from an upconversion of $P_{\mathrm{d}}^{(3)}(\omega)$ with another probe photon at the surface. The polarization $P_{\mathrm{d}}^{(4)}(2\omega)$ is of fourth order in the incident fields and dipole-forbidden in the bulk of centrosymmetric materials. In the experiment discussed below we are interested in only the dephasing time T_2 and not the relaxation time T_1, which arises from the finite lifetime of the excited carriers and their diffusion. In this case it is possible to work with two incident beams and use one of the pump pulses, e.g. E_{b}, simultaneously as a probe.

The observed self-diffracted signal is determined by

$$\boldsymbol{P}_{\mathrm{s}}^{(4)}\left(\boldsymbol{K}_{\mathrm{d}}^{(+1)}; 2\omega\right) = \chi_{\mathrm{s}}^{(4)} : \boldsymbol{E}_{\mathrm{a}}^{*}(\boldsymbol{k}_{\mathrm{a}})\boldsymbol{E}_{\mathrm{b}}^{3}(\boldsymbol{k}_{\mathrm{b}}) \tag{10}$$

$$K_{\mathrm{d},x}^{(+1)} = 2k_{\mathrm{b},x} + (k_{\mathrm{b},x} - k_{\mathrm{a},x})\,. \tag{11}$$

Its intensity $I_{\mathrm{d}}(2\omega) \propto |\boldsymbol{P}_{\mathrm{s}}^{(4)}(2\omega)|^2$ increases linearly with the intensity of pulse $\boldsymbol{k}_{\mathrm{a}}$ and with the third power of the intensity of pulse $\boldsymbol{k}_{\mathrm{b}}$. Its direction is given by (11) and the relationship $K_{\mathrm{d},x}^2 + K_{\mathrm{d},z}^2 = \epsilon\left(\frac{2\omega}{c}\right)^2$. There is also a self-diffracted 2ω signal in the same order radiating into the direction given by $K_{\mathrm{d},x}^{(-1)} = 2k_{\mathrm{b},x} - (k_{\mathrm{b},x} - k_{\mathrm{a},x})$. However, this signal is superimposed by the second-order sum-frequency response

$$\boldsymbol{P}_{\mathrm{s}}^{(2)}(\boldsymbol{K}_{\mathrm{SF}}; 2\omega) = \chi_{\mathrm{s}}^{(2)} : \boldsymbol{E}_{\mathrm{a}}(\boldsymbol{k}_{\mathrm{a}})\boldsymbol{E}_{\mathrm{b}}(\boldsymbol{k}_{\mathrm{b}}) \tag{12}$$

$$K_{\mathrm{SF},x} = k_{\mathrm{a},x} + k_{\mathrm{b},x}\,, \tag{13}$$

which will completely dominate the 2ω signal in this direction in the case of a weak grating.

2.2 *Excitation of* Si(111) 7×7 *dangling bonds*

For the discussion of the actual diffraction experiment it is useful to have some insight into the nature of the relevant electronic excitations and their influence on the nonlinear optical response. For this purpose we have performed pump–probe experiments at Si(111)7×7, using both 2PPE [45] and SHG [41]. The 2PPE investigations were conducted with the fundamental and frequency-tripled laser pulses of an amplified commercial Ti:sapphire laser (Quantronix RGA) operating at a wavelength of 800 nm and a repetition rate of 1 kHz. Pulse durations were 120 fs at the fundamental (IR) and 150 fs at the third-harmonic (UV) wavelength. Compared to the investigations of image-potential states, the role of UV and IR as pump and probe pulses is exchanged; the kinetic energy of the photoemitted electrons along the surface normal was measured by time-of-flight detection [45].

Figure 8 shows that the IR pump pulses produce an electron distribution above the Fermi level in the bulk band gap. The 2PPE intensity is seen to decay as a function of pump–probe delay with rates that depend on the energy above the Fermi level. Since the only allowed states in this energy region are due to the U_1 surface band, which arises from partially occupied adatoms of Si(111)7×7 [46], we attribute the observed feature to excitation of this band near the Γ point and the fast decay to redistribution of the electrons within the band due to electron–electron scattering [45].

It has been proposed that the unoccupied U_1 state is predominantly responsible for the observed resonant enhancement of SHG from Si(111)7×7 upon excitation with near infra-red laser light [47]. This state and the occupied dangling-bond-derived surface states S_1 and S_2 are quenched by most chemisorbates. In the frequency range from 750 to 1100 nm the nonlinear response is well described by a strong coverage-dependent term due to the dangling bonds $\chi_{\mathrm{s,db}}^{(2)}$ and a nonresonant contribution $\chi_{\mathrm{s,NR}}^{(2)}$ that is only weakly influenced by adsorption [47]

$$\chi_{\mathrm{s}}^{(2)}(\theta) \simeq \chi_{\mathrm{s,db}}^{(2)}(1 - \alpha\theta) + \chi_{\mathrm{s,NR}}^{(2)}(\theta)\,. \tag{14}$$

Figure 9 shows three different measurements of the SH signal as a function of the exposure with molecular oxygen. The fundamental light was provided by the same laser source as used in the IR light for the 2PPE experiments. The beam was split into a weak probe with a fluence of 1 mJ/cm^2 per pulse on the sample and a stronger pump beam of 14 mJ/cm^2. The beams were incident on the sample under different angles but without a time delay between the pulses.

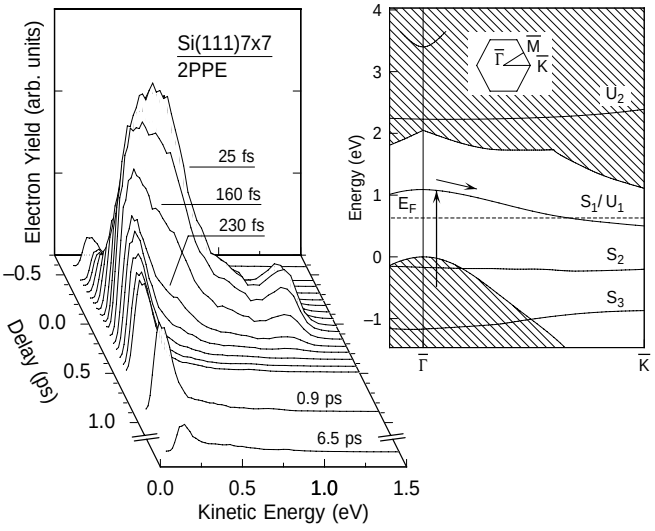

Fig. 8. *Left*: Transient electron population of usually unoccupied electronic states of Si(111)7×7 above the Fermi level ($E_{\mathrm{kin}} \simeq 0.25$ eV) generated by 1.55-eV pump pulses and detected by photoemission with 4.65-eV probe pulses for $k_{\parallel} \approx 0$. *Right*: Schematic band structure of Si(111)7×7 in an extended Brillouin zone with the excitation produced by the pump pulse and its relaxation indicated by arrows. S_1–S_3 and U_1, U_2 denote surface states; projected bulk states are hatched

Trace (b) is the reflected SH signal from the probe beam $\boldsymbol{k}_b$, with the pump $\boldsymbol{k}_a$ blocked. The signal first decreases as a function of oxygen exposure; there is a minimum for about 1 Langmuir, then the signal increases again and saturates at 20% of its initial value. This behavior is well understood from (14). The SH response of the clean surface is dominated by $\chi^{(2)}_{s,db}$. As more and more dangling bonds saturate as a result of oxygen exposure the signal decreases monotonously until the dangling-bond contribution becomes comparable with $\chi^{(2)}_{s,NR}$. A phase shift of about 160 degrees between both contributions, which are complex quantities, leads almost to a cancellation at an intermediate coverage. At high coverage all dangling bonds are quenched and the SH response is given by $\chi^{(2)}_{s,NR}$.

Trace (a) is the reflected SH signal from the pump beam $\boldsymbol{k}_a$. Here the minimum occurs for much smaller oxygen coverage and the response of the oxygen-saturated surface exceeds that of the clean surface. Very similar behavior is observed for the reflected SHG from the probe beam with the cross-polarized pump beam unblocked. Here, the strong electronic excitation of the U_1 band by the pump pulse that was directly observed in the 2PPE experiments reduces the relative strength of $\chi^{(2)}_{s,db}$ as compared to $\chi^{(2)}_{s,NR}$. This is expected for a resonantly enhanced SHG process with the U_1 band acting as an intermediate state [1]. The same effect is exploited in SFG experiments of vibrational energy relaxation [19, 42]. Experiments with delayed probe pulses show that the SH signal recovers on a timescale of 200 fs to 2 ps depending on the pump fluence. The corresponding incoherent scattering processes, characterized by a population decay time T_1, are not the subject of this paper [41].

Trace (d) corresponds to the SH signal of the probe beam self-diffracted in the direction $\boldsymbol{K}_d^{(+1)}$ when both *s*-polarized pump and probe beams are incident. The signal is 150 times weaker than the reflected SH signal of the probe beam (b) but still easily detectable. It decreases monotonously to zero as a function of oxygen exposure. The fact that this signal does not exhibit a minimum for intermediate oxygen exposures is important because it demonstrates that the main effect of the interfering pump and probe beams is indeed the generation of a population grating of the Si dangling bonds. Other possible excitations that might cause a spatial modulation of the SH efficiency appear to be weak.

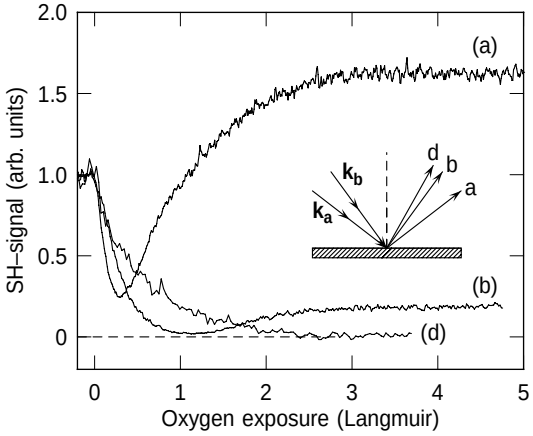

Fig. 9. Dependence of the SH signal from Si(111)7×7 on oxygen exposure generated by 100-fs pulses with fluences of 14 mJ/cm^2 (pump) and 1.0 mJ/cm^2 (probe). (a) Specular reflected SHG from the pump beam $\boldsymbol{k}_a$. (b) Reflected SHG from the probe beam $\boldsymbol{k}_b$ with the pump blocked. (d) Self-diffracted SH signal for parallel polarizations and zero delay of pump and probe beams. After an O_2 exposure of 5 Langmuir (1 Langmuir = $3.6 \times 10^{14} O_2$molecules/cm^2) all adatom dangling bonds are saturated at the surface temperature of 80 K [48]

The interpretation of SHG pump–probe experiments may be complicated by pump-induced changes of the bulk dielectric constant that effects the SHG process via Fresnel factors [39, 49–52]. This effect is negligible in the present experiments because of the weak absorption of silicon at a wavelength of 800 nm. If present, it would result in a spatial modulation not only of $\chi^{(2)}_{s,db}$ but also of $\chi^{(2)}_{s,NR}$. The diffracted SH signal would then be affected by the (destructive) interference of both contributions to the SH response which is not observed.

2.3 Dephasing of dangling-bond excitation

The pulse durations of 100–120 fs used for the above 2PPE and SHG experiments on Si(111)7×7 are too long for measurements of the extremely fast dephasing processes of the dangling-bond excitations. For these experiments we used a cavity-dumped Ti:sapphire system home-built after [53]. It delivers trains of IR pulses with durations below 15 fs and energies of 50 nJ at repetition rates up to 2 MHz. The pulses are split with a ratio of 3:7; the two beams are recombined on the sample at an angle of 2°. Prism pairs compensate for the broadening of the pulses in passing through the UHV entrance window and other dispersive elements in the beam paths. Interferrometric autocorrelation measurements show that the pulses at the end of the beam path are close to being transform-limited.

The SFG cross-correlation (12) from clean Si(111)7×7 measured with this set-up has a half-width of only 23 fs (Fig. 10a). Under the assumption of ideal sech^2 pulses this corresponds to a pulse duration of slightly less than 15 fs on the sample. The correlation trace of the diffracted signal (Fig. 10b) exhibits a sharper rise; it is asymmetric and its maximum is shifted to positive delay times. In the case of negligible dephasing time T_2 one would expect a symmetric distribution with half-width of 19 fs for the sech^2 pulses that produce the SFG signal of Fig. 10a. The best fit with variable finite decay time yields $\tau_d = 5.3 \pm 1$ fs.

Before we can discuss the physical relevance of the deduced time-constant τ_d we have to relate it to the dephasing time T_2. It also has to be explained why the finite response time of the system that is clearly visible in the diffracted signal (b) does not appear in the SFG signal (a). If the polarization $\boldsymbol{P}_a^{(1)}$ created by the pulse $\boldsymbol{k}_a$ is present when the delayed pulse $\boldsymbol{k}_b$ arrives at the surface, 2ω photons should be emitted. In fact, this has been exploited in IR-visible SFG experiments to measure the free induction decay of adsorbate vibrations [4, 5].

In the introduction to the transient grating experiment we assumed that the system is characterized by one resonantly excited transition frequency ω_{01}. In this case the polarization $\boldsymbol{P}_s^{(4)}$ would decay with a time constant T_2 and the measured diffracted signal $I_d \propto |\boldsymbol{P}_s^{(4)}|^2$ with $T_2/2$. However, this situation is not directly applicable to our experiment. The 7×7 structure of Si(111) is characterized by inequivalent

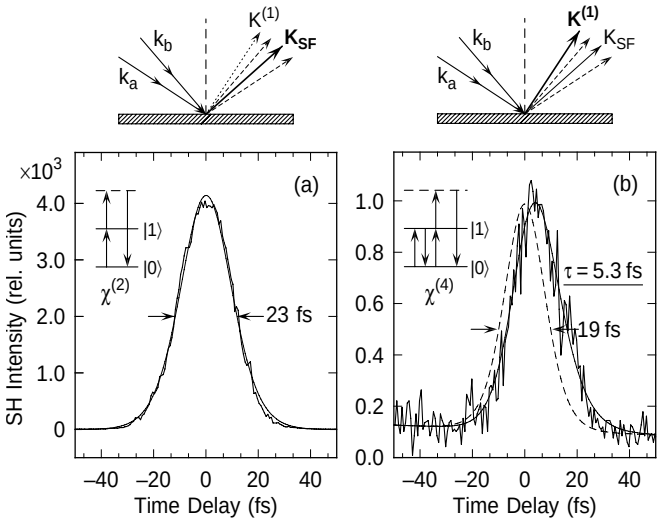

Fig. 10a,b. SFG cross-correlation (**a**) and self-diffracted SH signal (**b**) from two beams incident on a clean Si(111)7×7 surface under 22° and 24°. The *solid line* through the data of the cross-correlation (**a**) and the *dashed line* indicate the calculated response of sech^2 pulses with a full width at half maximum of 14.9 fs. The shift and asymmetric broadening of the diffracted signal corresponds to a decay time of 5.3 fs [54]

adatoms [46], the U_1 band has a width of several 100 meV (cf. Fig. 8), and the valence band provides a wide energy range for the initial states of excitation. Despite the short excitation pulses it is reasonable to assume that the inhomogeneous linewidth of the transition is larger than the spectral width of the pulse (~ 120 meV). Since the different excited eigenfrequency components evolve at different rates, $\mathrm{e}^{\mathrm{i}\omega_{01}t}$, the macroscopic polarization $\boldsymbol{P}_{\mathrm{a}}^{(1)}$ created by the first pulse will decay to zero within the pulse width, even in the absence of dephasing collisions. A delayed pulse $\boldsymbol{k}_{\mathrm{b}}$ cannot upconvert this polarization and generate 2ω radiation in the direction $K_{\mathrm{SF},x} = k_{\mathrm{a},x} + k_{\mathrm{b},x}$. In such a situation, small changes of the cross-correlation due to true dephasing processes are very difficult to detect even by means of interferometric measurements [55].

The diffracted signal, in contrast, is generated by a pulse sequence which causes transitions between $|0\rangle$ and $|1\rangle$. In this case the second pulse incident at $t = t_{\mathrm{b}}$ is able to reverse the phase evolution of the oscillating dipoles created by the first pulse at $t = t_{\mathrm{a}} = 0$. This leads to a so-called photon echo which is peaked at $t = 2t_{\mathrm{b}}$ [56]. In the present experiment the echo signal is not time-resolved. However, as its height is proportional to $\exp(-4t_{\mathrm{b}}/T_2)$ the echo leads to decay of the diffracted signal with a time constant $T_2/4$. The dephasing time corresponding to the decay time of ~ 5 fs is thus ~ 20 fs.

It must be emphasized that this is a preliminary result. For the precise determination of the dephasing time T_2 it will be necessary to take the interferometrically measured pulse shape and model the temporal evolution of the diffracted SH signal by means of a density matrix calculation. The observed decoherence time of 5 fs is shorter than the pulse duration of 15 fs. This fact ultimately limits the accuracy with which T_2 can be determined. In the present experiment, however, the simultaneous measurement of the SFG cross-correlation (a) guaranties that shift and asymmetry of the diffracted signal (b) are caused by a finite intrinsic time constant. The deduced number of $T_2 \sim 20$ fs is smaller than the dephasing times observed for free-carrier dephasing in bulk semiconductors or semicondcutor quantum wells [3] but larger than that of metallic systems [13]. Since the charge density in the dangling bonds of Si(111)7×7 is intermediate to those cases, this is the expected behavior.

3 Summary

Two different time-resolved surface spectroscopies that exploit coherence phenomena have been used to investigate the ultrafast dynamics of electrons in surface-specific electronic states.

Two-photon photoemission (2PPE) in combination with the coherent excitation of several quantum states was used to study image-potential states on metal surfaces. For a Cu(100) surface it was demonstrated that the spectroscopy of quantum beats makes previously unresolved high-order states (quantum number $n \geq 4$) experimentally accessible. By exciting electrons close to the vacuum level, electron wave packets could be created and detected that describe the quasi-classical periodic motion of weakly bound electrons.

A purely optical technique was employed for the investigation of dangling-bond excitations of Si(111)7×7. Two pulses of 15 fs duration were used to create a transient population grating. It was demonstrated that the finite dephasing time leads to an asymmetric temporal response of the self-diffracted second-harmonic signal. The five-wave-mixing process is characterized by a $\chi^{(4)}$ tensor. Like the $\chi^{(2)}$ processes SHG or SFG, it is dipole-forbidden in the bulk of centrosymmetric materials and should be applicable at many surfaces and interfaces. With the technique it is possible to deduce decay times for homogenously and inhomogenously broadened systems.

Acknowledgements. It is my great pleasure to thank the excellent co-workers who made this work possible. The image-potential states were investigated in collaboration with the group working with Th. Fauster, now located at the University of Erlangen. With U. Thomann, Ch. Reuß, I.L. Shumay and W. Wallauer we share the excitement of observing the first coherence effects with 2PPE. M. Kutschera and M. Weinelt joined the team in Erlangen and investigated defect-induced dephasing processes. The experiments on Si(111)7×7 were performed by W. Berthold, M. Mauerer and C. Voelkmann with support from I.L. Shumay and G.A. Schmitt. For the 2PPE measurements of this system we benefitted from a collaboration with P. Feulner, B. Kassühlke and D. Menzel from the Physics Department E20 at the TU München. The projects were generously supported by K.L. Kompa and are funded by the Deutsche Forschungsgemeinschaft through SFB 338.

References

1. Y.R. Shen: *The Principles of Nonlinear Optics* (Wiley, New York 1984)
2. W. Zinth, W. Kaiser: In *Ultrashort Laser Pulses – Generation and Applications*, 2nd ed., ed. by W. Kaiser, Topics Appl. Phys., Vol. 60 (Springer, Berlin, Heidelberg 1993) pp. 235–274
3. J. Shah: *Ultrafast Spectroscopy of Semiconductors and Semiconductor Nanostructures*, Springer Series in Solid-State Sciences, Vol. 115 (Springer, Berlin, Heidelberg 1996)
4. P. Guyot-Sionnest: Phys. Rev. Lett. **66**, 1489 (1991)
5. J.C. Owrutsky, J.P. Culver, M. Li, Y.R. Kim, M.J. Sarisky, M.S. Yeganeh, A.G. Yodh, R.M. Hochstrasser: J. Chem. Phys. **97**, 4421 (1992)
6. Y.M. Chang, L. Xu, H.W.K. Tom: Phys. Rev. Lett. **78**, 4649 (1997)
7. S. Ogawa, H. Nagano, H. Petek, A.P. Heberle: Phys. Rev. Lett. **78**, 1339 (1997)

8. H. Petek, A.P. Heberle, W. Nessler, H. Nagano, S. Kubota, S. Matsunami, N. Moriya, S. Ogawa: Phys. Rev. Lett. **78**, 4649 (1997)
9. J. Bokor: Science **246**, 1130 (1989)
10. R. Haight: Surf. Sci. Rep. **21**, 275 (1995)
11. M. Aeschlimann, M. Bauer, S. Pawlik: Chem. Phys. **205**, 127 (1996)
12. M. Wolf: Surf. Sci. **377-379**, 343 (1997)
13. H. Petek, S. Ogawa: Prog. Surf. Sci. **56**, 239 (1997)
14. N.-H. Ge, C.M. Wong, R.L. Lingle, Jr., J.D. McNeill, K.J. Gaffney, C.B. Harris: Science **279**, 202 (1998)
15. U. Höfer: Science **279**, 190 (1998)
16. U. Höfer, I.L. Shumay, Ch. Reuß, U. Thomann, W. Wallauer, Th. Fauster: Science **277**, 1480 (1997)
17. Ch. Reuß, I.L. Shumay, U. Thomann, M. Kutschera, M. Weinelt, Th. Fauster, U. Höfer: Phys. Rev. Lett. **82**, 153 (1999)
18. N. Bloembergen, R.K. Chang, S.S. Jha, C.H. Lee: Phys. Rev. **174**, 813 (1968)
19. Y.R. Shen: Annu. Rev. Phys. Chem. **40**, 327 (1989)
20. G.A. Reider, T.F. Heinz: In *Photonic Probes of Surfaces*, ed. by P. Halevi, Electromagnetic Waves: Recent Developments in Research, Vol. 2 (North-Holland, Amsterdam 1995) Chap. 8, pp. 3–66
21. P.M. Echenique, J.B. Pendry: J. Phys. C **11**, 2065 (1978); Prog. Surf. Sci. **32**, 111 (1990)
22. Th. Fauster, W. Steinmann: In *Photonic Probes of Surfaces*, ed. by P. Halevi, Electromagnetic Waves: Recent Developments in Research, Vol. 2 (North-Holland, Amsterdam 1995) Chap. 8, pp. 347–411
23. R.M. Osgood, Jr., X. Wang: Solid State Phys. **51**, 1 (1997)
24. R.W. Schoenlein, J.G. Fujimoto, G.L. Eesley, T.W. Capehart: Phys. Rev. B **43**, 4688 (1991)
25. T. Hertel, E. Knoesel, M. Wolf, G. Ertl: Phys. Rev. Lett. **76**, 535 (1996)
26. E.V. Chulkov, I. Sarria, V.M. Silkin, J.M. Pitarke, P.M. Echenique: Phys. Rev. Lett. **80**, 4947 (1998)
27. I.L. Shumay, U. Höfer, U. Thomann, Ch. Reuß, W. Wallauer, Th. Fauster: Phys. Rev. B **58**, 13 974 (1998)
28. W. Demtröder: *Laser Spectroscopy*, 2nd ed. (Springer, Berlin, Heidelberg 1991)
29. D.F. Padowitz, W.R. Merry, R.E. Jordan, C.B. Harris: Phys. Rev. Lett. **69**, 3583 (1992)
30. E.W. Plummer, W. Eberhardt: Adv. Chem. Phys. **49**, 533 (1982)
31. E.W. Plummer: Science **277**, 1447 (1997)
32. A. ten Wolde, L.D. Norrdam, A. Lagendijk, H. B. van Linden van den Heuvel: Phys. Rev. Lett. **61**, 2099 (1988)
33. J. Yeazell, M. Mallalieu, J. Parker, C.R. Stroud, Jr.: Phys. Rev. A **40**, 5040 (1989); J. Yeazell, M. Mallalieu, C.R. Stroud, Jr.: Phys. Rev. Lett. **64**, 2007 (1990)
34. G. Alber, P. Zoller: Phys. Rep. **199**, 231 (1991)
35. M. Nauenberg, C. Stroud, J. Yeazell: Sci. Am. **270**, 44 (June 1994)
36. E. Knoesel, A. Hotzel, M. Wolf: J. Electron Spec. Relat. Phenom. **88-91**, 577 (1998)
37. F. Theilmann, R. Matzdorf, A. Goldmann: Surf. Sci. **420**, 33 (1999)
38. M. Weinelt, Ch. Reuß, M. Kutschera, U. Thomann, I.L. Shumay, Th. Fauster, U. Höfer, F. Theilmann, A. Goldmann: Appl. Phys. B **68**, 377 (1999)
39. J. Hohlfeld, U. Conrad, E. Matthias: Appl. Phys. B **63**, 541 (1996)
40. J. Hohlfeld, E. Matthias, R. Knorren, K.H. Bennemann: Phys. Rev. Lett. **78**, 4861 (1996)
41. M. Mauerer, I.L. Shumay, U. Höfer: Phys. Rev. Lett. (submitted)
42. A.L. Harris, L. Rothberg: J. Chem. Phys. **94**, 2449 (1991)
43. J.A. Prybyla, H.W.K. Tom, G.D. Aumiller: Phys. Rev. Lett. **68**, 503 (1992)
44. A. Laubereau: In *Ultrashort Laser Pulses – Generation and Applications*, 2nd ed., ed. by W. Kaiser Topics in Applied Physics, Vol. 60 (Springer, Berlin, Heidelberg 1993) pp. 35–102
45. W. Berthold, M. Mauerer, U. Höfer, B. Kassühlke, P. Feulner: Solid State Commun., (to be published)
46. F.J. Himpsel: Surf. Sci. Rep. **12**, 1 (1990)
47. U. Höfer: Appl. Phys. A **63**, 533 (1996)
48. U. Höfer, P. Morgen, W. Wurth, E. Umbach: Phys. Rev. B **40**, 1130 (1989)
49. H.W.K. Tom, G.D. Aumiller, C.H. Brito-Cruz: Phys. Rev. Lett. **60**, 1438 (1988)
50. K. Sokolowski-Tinten, J. Bialkowski, D. von der Linde: Phys. Rev. B **51**, 14 186 (1995)
51. Y. Siegal, E.N. Glezer, E. Mazur: Phys. Rev. B **49**, 16 403 (1994)
52. I.L. Shumay, U. Höfer: Phys. Rev. B **54**, 15 878 (1996)
53. M.S. Pshenichnikov, W.P. de Boeij, D.A. Wiersma: Opt. Lett. **19**, 572 (1994)
54. C. Voelkmann et al.: (to be published)
55. M. Simon, F. Träger, A. Assion, B. Lang, S. Voll, G. Gerber: Chem. Phys. Lett. **296**, 579 (1998)
56. N.A. Kurnit, I.D. Abella, S.R. Hartmann: Phys. Rev. Lett. **13**, 567 (1964)